Mesoscale and macroscale kinetic energy fluxes from granular fabric evolution

David M. Walker and Antoinette Tordesillas*
Department of Mathematics and Statistics, University of Melbourne, Parkville, VIC 3010, Australia

Gary Froyland
School of Mathematics and Statistics, University of New South Wales, Sydney, NSW 2052, Australia
(Received 4 December 2013; published 21 March 2014)

Recent advances in high-resolution measurements means it is now possible to identify and track the local "fabric" or contact topology of individual grains in a deforming sand throughout loading history. These provide compelling impetus to the development of methods for inferring changes in the contact forces and energies at multiple spatiotemporal scales, using information on grain contacts alone. Here we develop a surrogate measure of the fluctuating kinetic energy based on changes in the local contact topology of individual grains. We demonstrate the method for dense granular materials under quasistatic biaxial shear. In these systems, the initially stable and solidlike response eventually gives way to liquidlike behavior and global failure. This crossover in mechanical behavior, akin to a phase transition, is marked by bursts of kinetic energy and frictional dissipation. Mechanisms underlying this release of energy include the buckling of major load-bearing structures known as force chains. These columns of grains represent major repositories for stored strain energy. Stored energy initially accumulates at all of the contacts along the force chain, but is released collectively when the chain overloads and buckles. The exact quantification of the buildup and release of energy in force chains, and the manner in which force chain buckling propagates in the sample (i.e., diffuse and systemwide versus localized into shear bands), requires detailed knowledge of contact forces. To date, however, the forces at grain contacts continue to elude measurement in natural granular materials like sand. Here, using data from computer simulations, we show that a proxy for the fluctuating kinetic energy in dense granular materials can be suitably constructed solely from the evolving properties of the grain's local contact topology. Our approach directly relates the evolution of fabric to energy flux and makes possible research into the propagation of failure from measurements of grain contacts in real granular materials.

DOI: 10.1103/PhysRevE.89.032205 PACS number(s): 81.05.Rm

I. INTRODUCTION

A proper understanding of how failure propagates spatially and temporally in granular materials is needed to ultimately mitigate and manage natural hazards, as well as minimize energy consumption or resource waste in particulate processes in industry [1–4]. A long-standing problem that has hampered research efforts is the lack of information at the microstructural level, *viz.,* at the scale of individual grains. While unprecedented high-resolution experimental measurements, achieved over the past decade, have steadily expanded the body of knowledge and insights into the processes at this scale, many key properties continue to elude measurement [4–7]. To capitalize on progress, robust analytical tools are needed to extract the most information from existing measurements across multiple spatial and temporal scales. A way forward is through the use of surrogate measures. The central idea is to predict the effect of a particular mechanism by tracking its influence on the surrogate, a property that can be measured—in place of the primary material property of interest that is difficult if not impossible to measure. For instance, the contacts and kinematics of individual grains of sand in a triaxial compression test can now be identified and tracked over many stages of loading [5–8]. However, forces at grain contacts in natural granular materials have so far eluded measurement. As such, the precise identification and tracking of key emergent structures such as force chains [9], and the quantification of energy fluxes into and out of these structures, remain unattainable.

Force chains play a central role in force transmission and energy flow in deforming granular systems [10–14]. These functional groups of grains bear the majority of the applied load and, in turn, serve as the main repositories for stored free energy [2,15–17]. Energy flow in and out of force chains is generally regulated by rearrangements among their laterally supporting neighbors. We recently found evidence that form and function go hand in hand in this process of self-organization [18,19], suggesting that some aspect of these rearrangements may provide a good surrogate for energy flow.

In Ref. [19], we studied the evolution of clusters comprising a particle and its contacting neighbors, in an experiment comprising circular photoelastic disks. We found favored cluster conformations, residing in distinct stability states in the structural stability landscape, which are reminiscent of "magic numbers" for molecular clusters. We also found that preferred conformational transitions are those that either preserve or increase the structural stability of the cluster. Clusters formed by particles in force chains reside in the more stable states of the stability landscape. This stability is provided by weak neighbors, which mobilize a dual resistance to buckling in a way that exploits all the benefits that topology can offer, *viz.,* neighbors in n-cycles laterally brace and prop up the column, and frustrate rotations through odd-cycle conformations [9,17,20,21]. Under increasing compression and shear, however, this resistance is ultimately overcome,

*atordesi@unimelb.edu.au

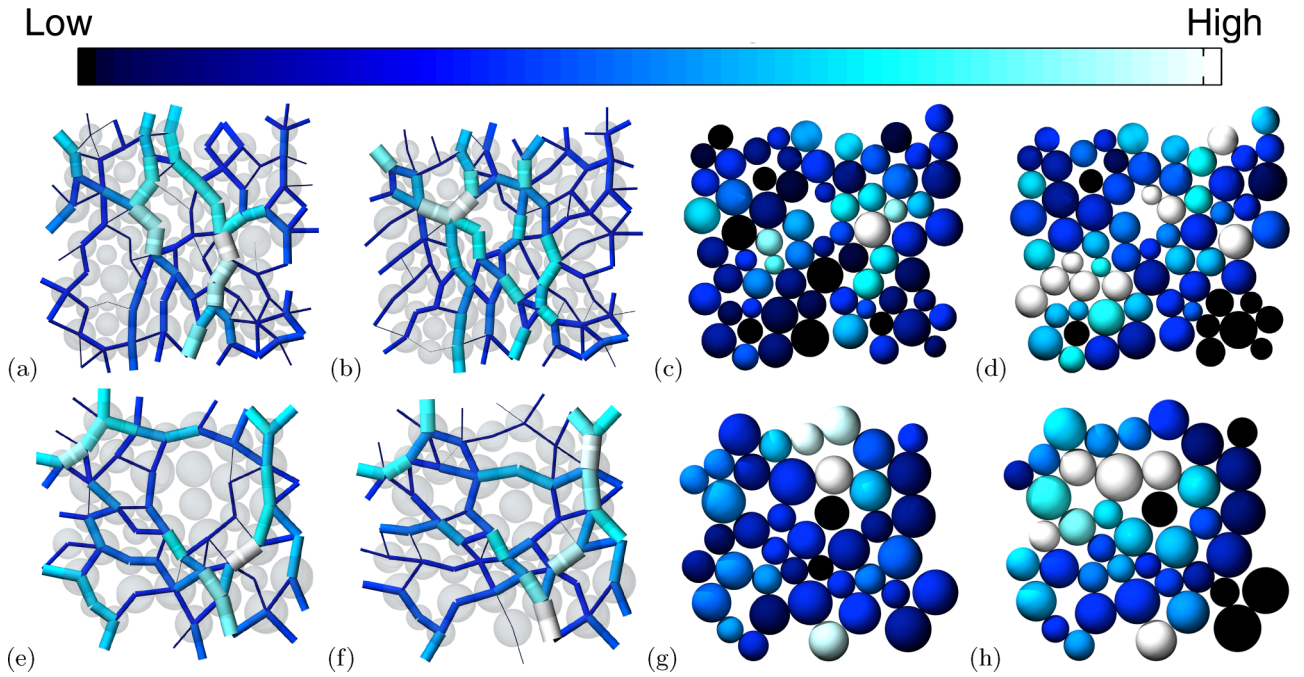

FIG. 1. (Color online) Change in local contact and contact force topology of a group of grains from computer simulations of biaxial compression under [(a)–(d)] constant confining pressure and [(e)–(h)] constant volume. Contacts are represented by bonds whose radius and color (dark to light) indicates the magnitude of the contact force (low to high) at the start [(a) and (e)] and end of a strain interval [(b) and (f)]. An increase (decrease) in contact force magnitude typically accompanies a local increase (decrease) in number of contacts or, alternatively, an increase (decrease) locally in lower (higher) length cycles. The change in the grain's contact forces is summarized in the change in the magnitude of its particle load vector magnitude [(c) and (g)]: The higher the change, the lighter the color. Our measure, which is based on contact topology alone, is shown in (d) and (h). Grain positions in (c) and (g) and (d) and (h) are at the end of the strain interval, identical to (b) and (f).

resulting in the collapse of the force chain by buckling. In Ref. [19], the most likely conformational transitions during buckling involve rearrangements among, or loss of, contacts which break the 3-cycle topology. The stored free energy, which is the potential elastic energy that was stored and accumulated at all the contacts along the force chain during the preceding stages, is then released collectively during buckling.

In sand experiments, the inability to identify force chains and their supporting neighbors makes it impossible to track this coordinated buildup and release of stored energy. Our approach seizes emerging opportunities from state-of-the-art experiments in granular micromechanics [5,6,8] and enables research into the spatiotemporal evolution of energy flow and failure propagation for geological materials. Answers to questions such as "How is the energy budget in a granular sample under load spatially and temporally distributed?" or "What structural rearrangements are responsible for energy dissipation?," which remain very difficult if not unattainable for natural materials, can now be undertaken at increasing levels of accuracy, concomittant with improvements in the temporal resolutions of measurement.

Specifically, in this paper, we propose a method that is based on the evolving contact topology alone—thus making the technique of value to state-of-the-art experimental measurements in dense granular media micromechanics [5,6,8]. The method is centered around a surrogate measure or proxy for the fluctuating kinetic energy so the mode of failure (i.e., localization or diffuse) may be tracked independently of knowledge of grains in force chains. To illustrate our idea, consider the topology of a group of grains in Fig. 1. The left column of Figs. 1(a) and 1(e) shows the contact topology of the grains from two biaxial compression tests. Across a strain interval, i.e., from Figs. 1(a) to 1(b) and from Figs. 1(e) to 1(f), the grains change position, contacts, and contact forces. One can clearly see the reconfigurations in the contact forces: this change includes the creation (loss) of bonds (or contacts), the increase (reduction) in bond strength (or contact force), and the inclusion or not of rattlers (or grains with no contacts) in the rearranged topology in Figs. 1(b) and 1(f). In the past [9], we used the "particle load vector" to summarize the contact forces acting on a given grain. The magnitude of this vector, λ_+, is derived as follows:

$$\lambda_+ = \frac{s_{11}+s_{22}}{2} + \sqrt{\left(\frac{s_{11}-s_{22}}{2}\right)^2 + s_{12}s_{21}}, \qquad (1)$$

where $s_{ij} = \sum_{c=1}^{N_c} n_i^{(c)} F_j^{(c)}$ denotes an effective force moment tensor per grain, N_c is the grain's coordination number, the superscript (c) stands for the cth contact, the subscripts i and j represent the ith and jth components of the unit normal vector $n_i^{(c)}$, and $F_j^{(c)}$ is a contact force vector [9]. The change in the particle load vector magnitude can be used as a measure of the reconfigurations in the contact forces of each grain [Figs. 1(c) and 1(g)]. Now, to presage our results, we show in Figs. 1(d) and 1(h) the results from one of our measures in this study that is based on information on contacts alone. Note that the

grains in Figs. 1(c) and 1(g) and Figs. 1(d) and 1(h) are in their final positions as are those in Figs. 1(b) and 1(f). Here the grains are colored light (dark) if they sustained large (small) changes with respect to the property in question, across the strain interval. It is convenient to partition the cluster into four quadrants. Comparing Figs. 1(a) and 1(b), one can see that the bottom left and top right quadrants of the cluster in Fig. 1(a) sustained force reconfigurations that are accompanied by marked changes in the local contact topology. Our measure in Fig. 1(d) captures this dynamics well, as shown by the light colors of the grains in these regions of the cluster. The same can be said for the top quadrants of the cluster in Fig. 1(e): here a strong "bridge" formed by the topmost grains weakens, giving way to a new "bridge" in Fig. 1(f) forming from the grains just below. Notice there is again a strong correlation between these reconfigurations in force and contact topology and the lightly colored grains in Fig. 1(h). By contrast, the measure provided by the particle load vector in Figs. 1(c) and 1(g) reflects only the most significant force reconfigurations, while changes in the local contacts bear only a secondary influence. This is evident in the dark colors of grains in the bottom left quadrant of the cluster in Fig. 1(c) and the left quadrants of the cluster in Fig. 1(g): These regions sustained marked changes in contact topology but not in contact forces. Note, however, that our measure is not directional: It does not distinguish between a change that involves an increase versus a decrease in connectivity. That is, loading up of stored energy due to gains in contacts is indistiguishable from off-loading, or release, of stored energy due to loss of contacts.

We will introduce our methods using two tests from a well-studied family of computer simulations [9] based on the methods in Ref. [22]. These samples consist of 5098 grains subject to biaxial compression and two different boundary conditions, namely constant confining pressure from the lateral boundaries (CP test) and constant volume (CV test) [9]. The grains are polydisperse spheres constrained to move in the plane and so the simulation is effectively two dimensional. The contact laws for two interacting grains is a combination of springs, dashpots, and sliders. A coefficient of rolling friction is introduced to a contact moment ($\mu^r = 0.02$) to better model the effects of grain shape seen in sand experiments [23]. Each sample exhibits multiphase response and a crossover from a solidlike to a liquidlike regime through the formation of a persistent shear band. In the constant confining pressure test, the shear band extends diagonally through the sample from the bottom left corner to the top right. The persistent shear band in the sample subject to constant volume boundary conditions forms a V shape but, at different temporal windows throughout the deformation, only one side of the V band is active. In both cases, the active bands also manifest a spatial interlacing of jammed and unjammed grains. The standard response behavior indicating each material's load-carrying capacity can be seen from the macroscopic stress ratio (Fig. 2). The transition to failure behavior is seen in the marked drop from peak stress ratio with increasing strain. The rises and drops in stress ratio can be attributed to stick-slip (jamming-unjamming) motion. Our interest in this paper is to track the evolution of the contact topology of each grain across strain intervals spanning stick-slip (jamming-unjamming) motion. Based on

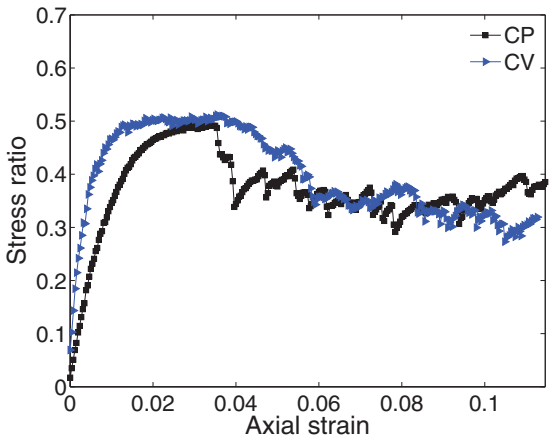

FIG. 2. (Color online) The macroscopic stress ratio with respect to increasing axial strain for the constant confining pressure test (CP black squares) and the constant volume test (CV blue triangles). Each test fails through strain localization and the formation of a persistent shear band at the time of the drop in stress ratio from peak.

how the local mesoscopic scale contact topology changes we introduce a proxy for fluctuating kinetic energy. In particular, by building on earlier work on mesoscopic cycle evolution [24,25], we show here how a spectral property of a network can also be used as an energy proxy measure. This means that a costly calculation of a networks' minimal cycle basis can be circumvented, further opening the method to greater practical use in real sands where hundreds of thousands of grains are the norm. Macroscopic averages of this quantity across the entire assembly of grains correlates strongly with the fluctuating kinetic energy [26–28], including nonaffine deformation measures that use full structural and kinematic information available in numerical experiments [9,29–32]. We argue that our method can be applied to the current state of experimental measurements where standard measures are not possible.

The remainder of this paper is organized as follows: In Sec. II we briefly summarize how changes in mesoscopic cycle topologies can be used to form a proxy for fluctuating kinetic energy across a strain increment. We also describe how the network spectral property of subgraph centrality can be used in place of full knowledge of the cycles in a network. The results of our methods and analysis when applied to the two test systems mentioned above are presented in Sec. III. We close the paper with a concluding discussion and speculate on the generality and suitability of our method in identifying sources of release of stored energy in real sands when only contact information is available.

II. CYCLE EVOLUTION AND AN ENERGY MEASURE

In computer simulations and also in experiments (e.g., photoelastic disks in 2D [14,33–36] and ID-Track in real 3D sand tests [5,6]) each grain and its contacts can be identified so the entire granular assembly can be represented by a complex network referred to as a contact network [37–40]. A complex network in simplest terms consists of a collection of nodes

which are connected by links. The structure of the network can be summarized by many properties across different scales. For example, locally, one can count the number of links associated to each node (i.e., the degree) or the number of contacting neighbors of a node that themselves are in contact with each other (i.e., triangles quantified by clustering coefficient). In addition to global averaging of these local properties at the macroscopic end of the scale, one can examine properties based on shortest path lengths (i.e., the minimum number of links which connect any pair of nodes). In a contact network each node represents an individual grain and a link between nodes exists if the corresponding grains are in mutual contact. In computer simulations and photoelastic disk experiments of shear and compression tests we have shown that the observed changes in rheology corresponds to evolving contact networks and their changing properties [39,41,42].

Structures within these networks are also of great importance to the rheology and of special import are the motifs associated to the (minimal) cycles in the network [43,44]. The cycles in a network are simply the closed paths in the network and geometrically can be described as the triangles, squares (quadrilaterals), pentagons, and so on. In 2D one can think of the minimal cycles of the contact network as the faces of a planar graph.

For a given observed strain state of the deformation, each grain and its associated network node is a member of a collection of cycles. We refer to any grain not in a cycle as a rattler and these grains are easily dealt with in our approach. We construct a vector summarizing this cycle topology whose elements are simply a count of the number and type of cycles associated to a node, i.e.,

$$C_t^i = [c_0, c_3, c_4, \ldots, c_n], \tag{2}$$

where, at strain t, node i has c_3 3-cycles, c_4 4-cycles, and up to c_n n-cycles in its local cycle topology. If node i is not in any cycle, then we set $c_0 = 1$ and $c_n = 0$, $n \geqslant 3$.

Consider, for example, a grain taken from the CP system as shown in Fig. 3. Across a strain interval of size Δt deformation leads to a change in its local cycle topology. At the start of the strain interval the local cycle topology of the identified grain can be represented by $C_t = [010011000]$ if we count up to $n = 10$ cycles. As we load the material further, grain rearrangements occur in response to the loading and a new strain will reveal a new fabric or contact topology. We can identify the same grain and construct a new vector summarizing its new cycle topology $C_{t+\Delta t}$. In Fig. 3 the new cycle vector is given by $C_{t+\Delta t} = [000110001]$, where again we count up to $n = 10$ cycles. We note that one local cycle, the 6-cycle, has remained intact over the interval, and the constituent grains of the 7-cycle have collapsed to form a 5-cycle but the largest change sees a 3-cycle cleaving to open a large dilatative region manifest as a 10-cycle.

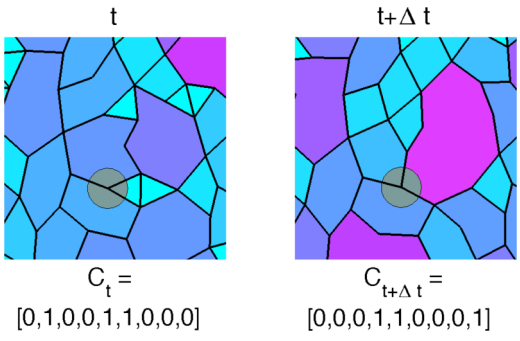

FIG. 3. (Color online) Quantifying the change in the local cycle topology of a grain across a strain interval Δt in the CP system. Cycles are colored by their size. At time t the grain is surrounded locally by one 3-cycle, one 6-cycle, and one 7-cycle. This local cycle topology changes to one 5-cycle, one 6-cycle, and one 10-cycle. The cosine distance between cycle vectors formed using these topologies is $d_C = 0.667$.

We can quantify this change by calculating the distance between these two vectors. Any distance norm will do but one which we have found revealing of the changing rheology is the cosine distance, i.e., the angle between the two vectors C_t and $C_{t+\Delta t}$. The cosine distance between two vectors x and y is

$$d_C(x,y) = 1 - \frac{x \cdot y^T}{\|x\|\|y\|}. \tag{3}$$

For a given node in the contact network this distance quantifies the evolving cycle topology over a strain interval. The local rearrangements in Fig. 3 return a d_C value of 0.6667. A measure of the average deformation of the entire assembly of N_p grains across a Δt increment of strain can also be obtained by

$$E_{CD}(\Delta t) = \frac{1}{N_p} \sum_{i=1}^{N_p} d_C\left(C_t^i, C_{t+\Delta t}^i\right). \tag{4}$$

We will show that when $\Delta t = 1$ this measure is a proxy for macroscopic fluctuating kinetic energy and qualitatively matches its evolution postpeak stress ratio in computer simulation tests. Furthermore, each individual $d_C(C_t^i, C_{t+\Delta t}^i)$ also spatially correlates with localized areas of energy release. That is, nodes with high (relative) values of $d_C(C_t^i, C_{t+\Delta t}^i)$ correspond to grains residing in the shear band and also to neighborhoods of force chain failure events. We thus argue that identifying the nodes with a high value of $d_C(C_t^i, C_{t+\Delta t}^i)$ in the evolving contact topology of dense granular assemblies reliably locates the zones of failure, deformation, and energy release postpeak without the need for additional force information.

A. Subgraph centrality

The framework described above relies on the determination of the minimal cycle basis of the network [43,44]. The information used for each node is the local minimal cycle topology, i.e., higher length cycles are not included if they consist of combinations of lower length cycles. For example, consider a 4-cycle which is made up of two 3-cycles sharing a link. Such a cycle would not be a part of a minimal cycle basis and so would not be considered in the local mesoscopic cycle evolution framework described above. It is useful, however, to consider a measure of cycle topology whose extent goes beyond the mesoscopic scale. For example, consider a grain that resides in a densely packed area of the assembly, strongly supported by contacting first ring of neighbors; however,

these neighbors due to (possible) dilatative rearrangements are poorly supported on the other side. The cycle vector construction described above would "not see" these areas of dilatation at this mesoscopic scale of the second ring of neighbors. A measure which (implicitly) includes this additional level of information by accounting for cycles at larger scales and also nonminimal cycles such as the 4-cycle described above is subgraph centrality [45–47].

Subgraph centrality is a network node property which quantifies the number of closed walks within the network that a node is involved in. This includes all minimal n-cycles as well as larger cycles which are not minimal. The property is weighted with shorter length cycles given the most weight. This means the essential local mesoscopic scale cycle topologies are given importance but larger-scale dilative configurations are also included. A node with a local cycle topology consisting of many short cycles—a densely packed or jammed region of the material—has a larger subgraph centrality index than a node in a less densely packed area of the material.

The calculation of subgraph centrality depends on the spectral properties of the adjacency matrix [45]. Mathematically, the diagonal entries of A^n (nth power of an adjacency matrix) gives the number of closed paths of length n starting and ending at a particular node. This count includes all of the minimal n-cycles involving a node. The measure of subgraph centrality quantifies this by considering for node i the following:

$$S^i = \sum_{k=0}^{\infty} \frac{\mu_k(i)}{k!}, \tag{5}$$

where $\mu_k(i) = (A^k)_{ii}$. Each S^i can be expressed in terms of the spectral structure of the adjacency matrix A [45],

$$S^i = \sum_{j=1}^{N_p} \left(v_j^i\right)^2 e^{\lambda_j} \tag{6}$$

for N_p nodes and eigenvalues λ_j and with v_j^i being the ith component of the jth (orthonormal) eigenvector.

We can build an equivalent proxy for fluctuating kinetic energy (say, E_{SCD} miming Eq. (4)) by following the same framework above for local minimal cycles but instead using changes in subgraph centrality. That is, we replace C_t^i and $C_{t+\Delta t}^i$ in Eq. (4) with S_t^i and $S_{t+\Delta t}^i$ respectively to define

$$E_{SCD}(\Delta t) = \frac{1}{N_p} \sum_{i=1}^{N_p} d_E\left(S_t^i, S_{t+\Delta t}^i\right), \tag{7}$$

where using a Euclidean norm seems more appropriate in this case. This new measure not only contains information of local mesoscopic cycle rearrangements but also information of global cycle changes and their relevance to particular nodes.

B. Energy measures in granular assemblies

We test our claim that the score given in Eq. (4) and the version using subgraph centrality in Eq. (7) can be considered a proxy for energy loss in a network by comparing our scores to two measures of energy dissipation in the assembly. This is possible for our systems as additional knowledge beyond network structure is available in computer simulations. In other applications and systems where these more standard measures of energy are unavailable we hope our network quantity can be a useful proxy. The first corroboration is to compare our scores to the strain evolution of the macroscopic energy, in particular, the fluctuating kinetic energy of the whole assembly [26–28]. That is,

$$E_f = \sum_{i=1}^{N_p} \left(\frac{m(|v^i| - \langle |v^i| \rangle)^2}{2} \right), \tag{8}$$

where, as before, N_p is the number of grains in the assembly and v^i is the velocity (effectively displacement) of each grain (mass m) across an interval of strain [9]. The brackets indicate the average fluctuating velocity across the entire assembly.

A second comparison is to the nonaffine strain which is a measure of the observed deviation of a grain cluster from that expected if the deformation was solely attributable to the affine strain tensor [9,29–32,48]. A scalar measure of the nonaffine deformation for each grain cluster can be calculated and averaged over the whole assembly to obtain a macroscopic measure [9,30]. Specifically, consider a reference grain and its set B of neighboring grains as determined by Delauney polygons of total volume V emanating from the reference grain. The edges of these polygons define branch vectors $\mathbf{l}^c$ with components l_j^c from the reference grain to each $c \in B$. If $\mathbf{u}$ denotes the displacement of the reference grain and $\mathbf{u}^c$ denotes the displacements of each grain $c \in B$, then the relative displacement of the cth neighbor in relation to the reference grain is given in components by

$$p_i^c = u_i^c - u_i + e_{ij3} l_j^c \omega, \tag{9}$$

where ω is the angle of rotation of the reference grain, e_{ijk} is the Levi-Civita symbol, and repeated indices are summed over. The p_i^c are used to define an approximation to the affine strain tensor based on the observed grain motion, i.e.,

$$\varepsilon_{ij} = \frac{1}{2V} \sum_{c \in B} \left(p_i^c - p_i^{c+1}\right) e_{jk3} \left(l_k^{c+1} - l_k^c\right). \tag{10}$$

A scalar measure for the nonaffine deformation associated with the deformation of a grain cluster with respect to a reference grain is

$$\Delta^\varepsilon = \frac{1}{2V} \sum_{c \in B} |\Delta \mathbf{p}^c| (|\mathbf{l}^{c+1} - \mathbf{l}^c| + |\mathbf{l}^c - \mathbf{l}^{c-1}|), \tag{11}$$

where $\Delta \mathbf{p}^c = \mathbf{p}^c - \varepsilon \cdot \mathbf{l}^c$ is the difference between the actual relative displacement in Eq. (9) and that implied by the affine strain tensor from Eq. (10). Equation (11) can be averaged over each grain in the assembly to obtain a macroscopic measure of the nonaffine deformation we denote with E_{NA}. It has been shown that these measures temporally and spatially correlate with energy loss in the system as well as known dissipative mechanisms such as microbands and force chain buckling [9].

III. RESULTS

In this section we will first show that the measure defined in Eq. (4), and its subgraph centrality alternative Eq. (7),

TABLE I. Pearson coefficient of the temporal correlation of E_{CD} and E_{SCD} dissipation measures with fluctuating kinetic energy (E_f) and nonaffine deformation (E_{NA}) values postpeak stress ratio.

	E_{CD}		E_{SCD}	
Test	E_f	E_{NA}	E_f	E_{NA}
CP	0.85	0.96	0.83	0.95
CV	0.88	0.95	0.88	0.95

exhibits strong temporal correlation with a more standard measure of fluctuating kinetic energy Eq. (8) and the nonaffine deformation measure in the postpeak stress ratio failure regime of both samples. We measure the strength of correlation using the Pearson correlation coefficient given for two sets of data $\{x_i\}_{i=1}^n$ and $\{y_i\}_{i=1}^n$ by

$$r = \frac{\sum_{i=1}^n (x_i - \mu_x)(y_i - \mu_y)}{\sqrt{\sum_{i=1}^n (x_i - \mu_x)^2}\sqrt{\sum_{i=1}^n (y_i - \mu_y)^2}}, \qquad (12)$$

where μ_x and μ_y are the sample means of $\{x_i\}_{i=1}^n$ and $\{y_i\}_{i=1}^n$, respectively. The strength of the correlation between E_{CD} or E_{SCD} with these more standard measures is high for both test systems with different boundary conditions as seen in Table I. The temporal traces in Fig. 4 highlight the strength of these correlations with both measures capturing the spiking nature of both the kinetic energy and nonaffine deformation measures during drops in stress ratio. Our proxy for energy loss using all of the local cycles, i.e., E_{CD}, shows a slightly stronger correlation than the proxy calculated using subgraph centrality (E_{SCD}). The drop in performance does not appear to be too great considering the benefit of a less-demanding subgraph centrality calculation.

We note that prepeak stress ratio our proxies E_{CD} and E_{SCD} exhibit a poor performance when compared to E_f and E_{NA}. Prepeak we observe fluctuations of E_{CD} and E_{SCD} around residual values. These residual values are higher than observed in the more standard energy measures. This discrepancy can partially be attributed to the nondirectionality of our cycle topology measures. That is, topological changes which lead to a loading-up of stored energy at contacts, e.g., a 4-cycle compressing to become two 3-cycles, is indistinguishable from two 3-cycles cleaving to form one 4-cycle in an energy off-loading mechanism. Both sets of rearrangements contribute the same to our energy proxy, thus the prepeak behavior of the compressed assembly is being captured. Standard energy measures based on grain motion would only register if these "loading-up" rearrangements were accompanied by a large movement of grains which is not typical during the early stages of compression. A second contributing factor during this prepeak regime are dilatative rearrangments. We know from earlier studies [39,42] that 3-cycles in particular are degrading during strain hardening. Our energy proxy is also capturing these changes, regardless of whether they are accompanied by greater movement of grains, thus contributing to the higher residual value before failure. Postpeak stress ratio the large bursts in kinetic energy are well captured, and these bursts accompany a drop in stress ratio, attributable to the failure mechanism of force chain buckling.

In addition to strong temporal correlations our proxies also exhibit a degree of spatial correlation with known zones of deformation in the sample over strain intervals where major grain rearrangements have occurred. For example, in Figs. 5(a) and 5(c) we present the constant confining pressure test assembly, with grains colored according to low and high values of the individual terms in E_{CD} and E_{SCD}, i.e., $d_C(C_t^i, C_{t+\Delta t}^i)$ and $d_E(S_t^i, S_{t+\Delta t}^i)$, respectively. These values are calculated across a strain interval during the drop from peak stress ratio and are typical for strain intervals spanning

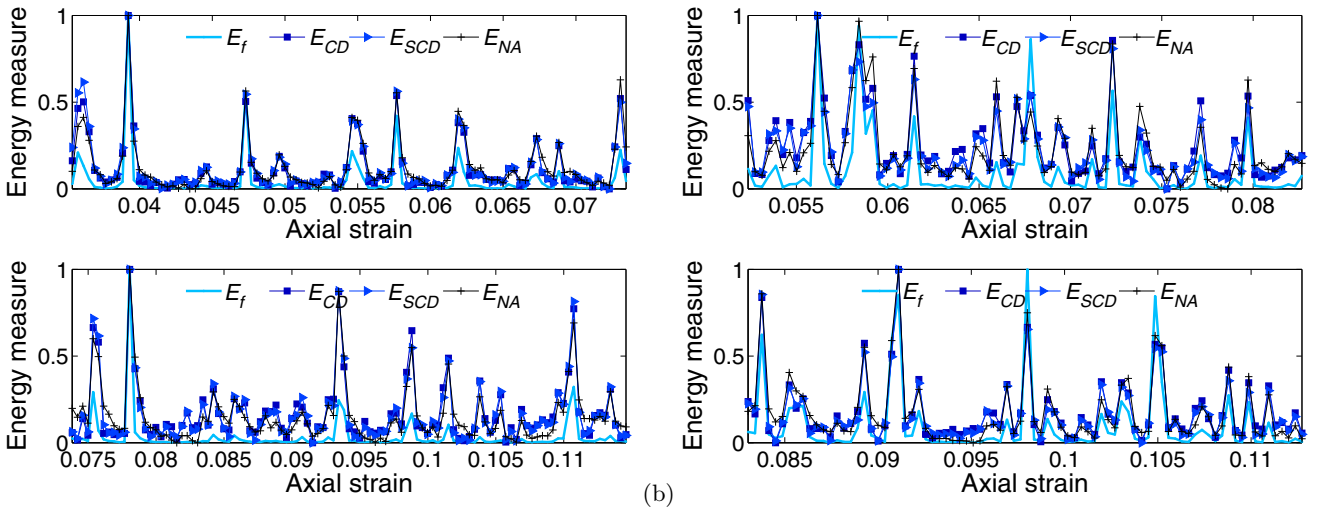

FIG. 4. (Color online) Temporal correlation between fluctuating kinetic energy (E_f) and nonaffine deformation (E_{NA}) with our proposed proxies for energy dissipation E_{CD} and E_{SCD}. All energy measures have been rescaled independently to lie in the range [0,1] for better visualization of the simultaneous spiking. Traces are plotted for the postpeak stress ratio regime in both samples with the upper plots displaying the first half of these regimes and the lower plots the second half for improved clarity. (a) Constant confining pressure test. (b) Constant volume test.

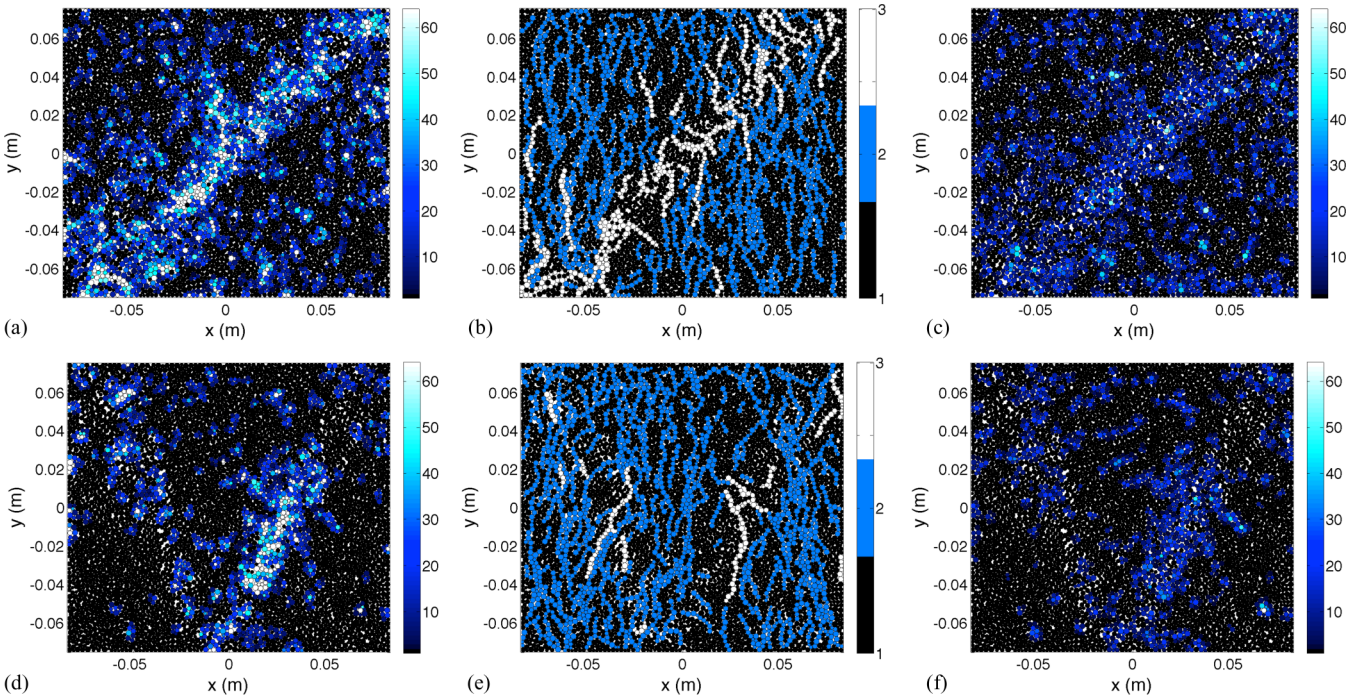

FIG. 5. (Color online) Constant confining pressure test (a) spatial visualization of $d_C(C_t^i, C_{t+\Delta t}^i)$ over a strain interval corresponding to a drop in stress ratio following peak stress ratio. (b) Across the same interval a plot of the strong force chain network (color 2), the weak network (color 1), and those chains which fail by buckling across the interval (color 3). (c) As in (a) but showing a spatial visualization of $d_E(S_t^i, S_{t+\Delta t}^i)$. Constant volume test (d) spatial visualization of $d_C(C_t^i, C_{t+\Delta t}^i)$ over a strain interval corresponding to a large drop in stress ratio well into the high-strain regime. (e) Across the same interval a plot of the strong force chain network (color 2), the weak network (color 1), and those chains which fail by buckling across the interval (color 3). (f) As in (d) but showing a spatial visualization of $d_E(S_t^i, S_{t+\Delta t}^i)$. Values of $d_C(C_t^i, C_{t+\Delta t}^i)$ and $d_E(S_t^i, S_{t+\Delta t}^i)$ in (a), (c), (d), and (f) are scaled to lie in the range [1,64] to better contrast low and high values.

a drop in stress ratio postpeak. One can see that high values of both $d_C(C_t^i, C_{t+\Delta t}^i)$ and $d_E(S_t^i, S_{t+\Delta t}^i)$ localize in what is the shear band region (lightly colored particles). In Fig. 5(b) the weak network, strong force chain network and those force chains that have failed by the energy releasing mechanism of buckling across the same interval are plotted. Force chains and those which buckle across a strain interval are identified using established algorithms [49]. Grains in force chains have above-average particle load vector magnitude determined by Eq. (1). A sequence of three or more of these grains in contact and quasilinear alignment with respect to the associated eigenvector of Eq. (1) identifies a force chain. Grains not in force chains are classified here as members of the weak network. A buckled force chain can be identified as a force chain at the beginning of a strain interval experiencing a drop in particle load vector magnitude of its constituent grains by the end of the strain interval and also a loss of quasilinear alignment in any contiguous three-grain segments of the chain. A visual inspection confirms that in the vicinity of buckling force chains our energy proxies register high values. The situation for the constant volume test is similar as shown in Figs. 5(d), 5(e), and 5(f). In this CV test the shear band forms a V shape with the right wing particularly active during the presented strain interval. In Fig. 6 we show [Fig. 6(a)] the observed displacement field, Fig. 6(c)] the nonaffine displacement field, and [Fig. 6(b)] the nonaffine deformation measure for the constant confining pressure test. Comparing with the panels in Fig. 5 we see that our cycle energy measure obtained solely from the evolution of the contact network cycle topology spatially coincides with measures dependent on particulate displacements and also local cluster topology changes. The constant volume test exhibits analogous correspondence in features as shown in Figs. 6(d), 6(e), and 6(f).

These results and observations are consistent with current thinking on the dynamics of shear bands. Mechanisms that act counter to the macroscopic trend, i.e., grains that load up (off-load) when stress ratio drops (increase), must always be confined to the shear band. Our methods are nondirectional as changes due to processes which load up (e.g., local compaction or jamming associated with higher length cycles collapsing to lower length cycles) or off-load (e.g., local dilatation or unjamming where lower length cycles cleave to become higher length cycles) are not distinguished. Since the highest changes in our measures are predominently confined to the shear band, we are seeing confirmation of current opinion. The regions outside the shear band simply reflect the physics of the dominant mechanism in the shear band. Sometimes there is a clear dominant mechanism (clear rise or drop in stress ratio) and sometimes not (competing events are almost balanced), and so any method that can hone in on the zone where such activity is occurring using information currently available from real experiments—as our method does—is of value.

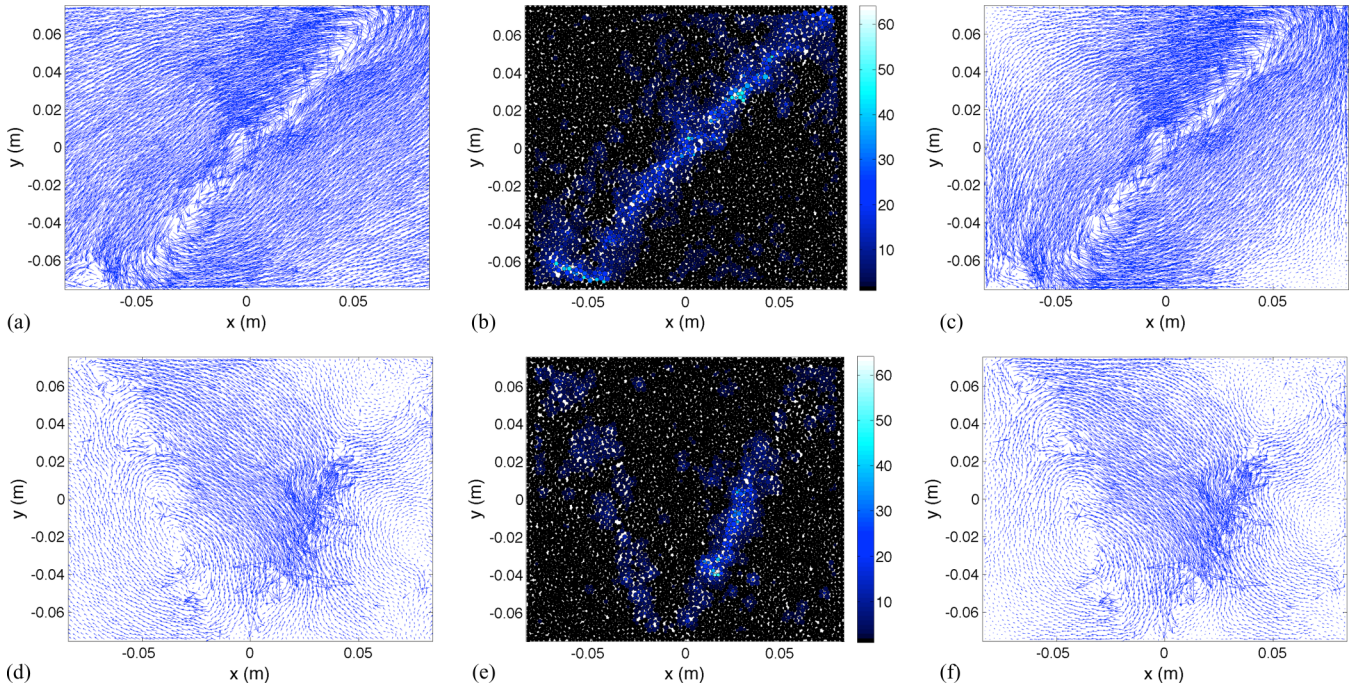

FIG. 6. (Color online) Constant confining pressure test. (a) The observed grain displacement field over the same interval in (Fig. 5). (b) Spatial visualization of the incremental nonaffine measure. (c) The nonaffine grain displacement field, i.e., the displacement field obtained by subtracting the motion of the boundary walls from the observed displacement field. Constant volume test [(d), (e), and (f) as (a), (b), and (c)]. Values of the incremental nonaffine measure are scaled to lie in the range [1,64] to better observe the contrast of low and high values. The vectors of the displacement field are scaled by a constant factor to better show the regions of activity.

IV. CONCLUSION

Understanding how failure propagates spatially and temporally in granular materials is key to our ability to control a broad gamut of natural and human-made processes. To achieve this, tools must be developed that can track energy storage and dissipation at the particulate level and relate these local processes to macroscopic behavior. Here we take steps in developing such tools, spurred by the recent progress in high-resolution measurements, which enable individual grain contacts to be identified and tracked for many stages of the loading history. We developed a surrogate measure for the fluctuating kinetic energy based on contact information alone. This surrogate measure is simple and quantifies the evolving local cycle topology of a network node—using the exact local cycle basis topology [44] or the network spectral property of subgraph centrality [45]. We demonstrated that the temporal and spatial evolution of failure zones and possible sites of force chain buckling can be identified using this surrogate measure, leading to the possibility of the same phenomena being pinpointed in sand samples without the need for measurements on contact forces.

Ongoing efforts are focused on the application of this method to characterize the propagation of failure in both 2D and 3D systems for a range of real materials (e.g., sand, synthetic materials comprising photoelastic disks, and hydrogel spheres), as well as in grain simulations. More accurate methods to prise the essential processes governing the spatial and temporal propagation of energy calls for directionality (i.e., the capability to distinguish loading-up verses off-loading of stored energy at contacts). This suggests an approach along the lines of a Perron-Frobenius eigenvalue calculation using different cycle vectors and matrices which capture the evolution of probabilities. This is beyond the scope of the present formalism but is currently under investigation.

Finally, it is interesting to compare the systems studied here comprising spherical particles (confined to move in a plane) with the assemblies in Azema *et al.* [50] comprising polyhedral particles. In the latter, the influence of contact topology or fabric is more subdued. This is due to the faceted particles forming highly stable, edge-to-edge contacts. These contacts can build up much higher forces and, in turn, store larger amounts of potential elastic energy than would otherwise be possible for near-point contacts in assemblies of spherical particles or circular disks. We therefore expect the current metric which solely focuses on contact topology to be less effective for systems comprising irregularly shaped or elongated faceted particles that can form highly stable contacts. For these systems, we envisage a different network and possibly a new network metric, which takes into account *both* contact topology and contact shape. One way to do this is to consider a weighted contact network, where the weight assigned to each link depends on the associated area of contact, keeping in mind that the links in the network represent the contacts between the particles in the granular sample.

ACKNOWLEDGMENTS

We thank our anonymous reviewers for their useful suggestions, which have improved this paper. This work was supported by the US Army Research Office (Grant

No. W911NF-11-1-0175), the Australian Research Council Discovery Projects 2012 (Grant No. DP120104759), and the Melbourne Energy Institute. G.F. was supported by an ARC Future Fellowship (FT120100025).

[1] B. Carson and P. L. Berglund, Geol. Soc. Am. Mem. **166**, 135 (1986).
[2] A. Ord, B. Hobbs, and K. Regenauer-Lieb, Int. J. Numer. Anal. Met. **31**, 373 (2007).
[3] P. W. Cleary, R. C. Z. Cohen, S. M. Harrison, M. D. Sinnott, M. Prakash, and S. Mead, Eng. Comput. **30**, 157 (2013).
[4] G. Michlmayr, D. Cohen, and D. Or, Earth-Sci. Rev. **112**, 97 (2012).
[5] S. Hall, M. Bornert, J. Desrues, Y. Pannier, N. Lenoir, G. Viggiani, and P. B'esuelle, Geotechnique **60**, 315 (2010).
[6] E. Andò, S. A. Hall, G. Viggiani, J. Desrues, and P. Bésuelle, Acta Geotech. **7**, 1 (2012).
[7] M. B. Cil and K. A. Alshibli, Geotech. Lett. **2**, 161 (2012).
[8] A. Tordesillas, D. M. Walker, E. Andò, and G. Viggiani, Proc. R. Soc. A **469**, 20120606 (2013).
[9] A. Tordesillas, Philos. Mag. **87**, 4987 (2007).
[10] P. Dantu, Geotechnique **18**, 50 (1968).
[11] A. Drescher and G. de Josselin de Jong, J. Mech. Phys. Solids **20**, 337 (1972).
[12] M. Oda, T. Takemura, and M. Takahashi, Geotechnique **54**, 539 (2004).
[13] M. Oda and H. Kazama, Geotechnique **48**, 465 (1998).
[14] T. Majmudar and R. Behringer, Nature **435**, 1079 (2005).
[15] J. F. Peters, M. Muthuswamy, J. Wibowo, and A. Tordesillas, Phys. Rev. E **72**, 041307 (2005).
[16] S. D. C. Walsh, A. Tordesillas, and J. F. Peters, Granul. Matter **9**, 337 (2007).
[17] G. W. Hunt, A. Tordesillas, S. C. Green, and J. Shi, Phil. Trans. R. Soc. A **368**, 249 (2010).
[18] A. Tordesillas, Q. Lin, J. Zhang, R. P. Behringer, and J. Shi, J. Mech. Phys. Solids **59**, 265 (2011).
[19] A. Tordesillas, D. M. Walker, G. Froyland, J. Zhang, and R. P. Behringer, Phys. Rev. E **86**, 011306 (2012).
[20] A. Tordesillas and M. Muthuswamy, J. Mech. Phys. Solids **57**, 706 (2009).
[21] A. Tordesillas, J. Zhang, and R. P. Behringer, Geomech. Geoeng. **4**, 3 (2009).
[22] P. A. Cundall and O. D. L. Strack, Geotechnique **29**, 47 (1979).
[23] N. Estrada, E. Azema, F. Radjai, and A. Taboada, Phys. Rev. E **84**, 011306 (2011).
[24] D. M. Walker, A. Tordesillas, and G. Froyland, Nonlinear Theor. Appl. **4**, 148 (2013).
[25] D. M. Walker, A. Tordesillas, and G. Froyland, in *2012 International Symposium on Nonlinear Theory and its Applications, Palma, Majorca, Spain, October 22–26, 2012* (Research Society of Nonlinear Theory and its Applications, IEICE, Japan, 2012), http://www.ieice.org/ess/nolta/2012/.
[26] C. Thornton and L. Zhang, Philos. Mag. **86**, 3425 (2006).
[27] F. Nicot, L. Sibille, and F. Darve, Int. J. Plastic. **29**, 136 (2012).
[28] J. F. Peters and L. E. Walizer, J. Eng. Mech-ASCE **139**, 1479 (2013).
[29] J. F. Peters, J. Eng. Math. **52**, 231 (2005).
[30] A. Tordesillas, M. Muthuswamy, and S. D. C. Walsh, J. Eng. Mech-ASCE **134**, 1095 (2008).
[31] K. C. Valanis and V. P. Panoskaltsis, Acta Mech. **175**, 77 (2005).
[32] M. Griffa, E. G. Daub, R. A. Guyer, P. A. Johnson, C. Marone, and J. Carmeliet, Europhys. Lett. **96**, 14001 (2011).
[33] J. Zhang, T. S. Majmudar, A. Tordesillas, and R. P. Behringer, Granul. Matter **12**, 159 (2010).
[34] T. S. Majmudar, M. Sperl, S. Luding, and R. P. Behringer, Phys. Rev. Lett. **98**, 058001 (2007).
[35] D. Bi, J. Zhang, B. Chakraborty, and R. P. Behringer, Nature **480**, 355 (2011).
[36] J. Ren, J. A. Dijksman, and R. P. Behringer, Phys. Rev. Lett. **110**, 018302 (2013).
[37] A. Smart and J. M. Ottino, Soft Matter **4**, 2125 (2008).
[38] R. Arévalo, I. Zuriguel, and D. Maza, Int. J. Bifurcat. Chaos **19**, 695 (2009).
[39] D. M. Walker and A. Tordesillas, Int. J. Solids Struct. **47**, 624 (2010).
[40] R. Arévalo, I. Zuriguel, and D. Maza, Phys. Rev. E **81**, 041302 (2010).
[41] A. Tordesillas, D. M. Walker, G. Froyland, J. Zhang, and R. P. Behringer, Phys. Rev. E **86**, 011306 (2012).
[42] A. Tordesillas, D. M. Walker, and Q. Lin, Phys. Rev. E **81**, 011302 (2010).
[43] J. D. Horton, SIAM J. Comput. **16**, 358 (1987).
[44] K. Mehlhorn and D. Michail, J. Exp. Algorithm. **11**, 1 (2006).
[45] E. Estrada and J. A. Rodríguez-Velázquez, Phys. Rev. E **71**, 056103 (2005).
[46] E. Estrada and J. A. Rodríguez-Velázquez, Phys. Rev. E **72**, 046105 (2005).
[47] E. Estrada and N. Hatano, Chem. Phys. Lett. **439**, 247 (2007).
[48] A. Tordesillas, D. Kirszenblat, and C. Mangelsdorf, Australas. J. Eng. Educ. **15**, 85 (2009).
[49] M. Muthuswamy and A. Tordesillas, J. Stat. Mech.: Theory Exp. (2006) P09003.
[50] E. Azéma, F. Radjaï, and F. Dubois, Phys. Rev. E **87**, 062203 (2013).